

Second harmonic generation by radially polarized laser beam propagating in homogeneous plasma

Shivani Aggarwal¹, Dinkar Mishra¹, Saumya Singh¹, Bhupesh Kumar^{1*}, Pallavi Jha^{1,2}

¹*Department of Physics, University of Lucknow, Lucknow (U.P.) – 226007, India*

²*Retired Professor*

**Corresponding author: bhupeshk05@gmail.com*

Abstract

This study presents an investigation of second harmonic generation (SHG) resulting from interaction of radially polarized laser beam propagating in homogeneous, unmagnetized plasma. Lorentz force and continuity equations have been used to derive the radial and axial current density components. Further, using these densities in the wave equation leads to analytical expressions for the SHG field amplitudes. These amplitudes exhibit periodic oscillations along the propagation axis, characterized by detuning length dependent on plasma density and laser parameters. Radial and axial contributions to SHG are found to be highly enhanced near the beam axis due to the Gaussian beam profile of the laser. The analytical findings are validated using Fourier Bessel Particle-In-Cell (FBPIC) simulations. Notably, unlike linearly or circularly polarized beams which require either inhomogeneous or magnetized plasma, radially polarized beams facilitate efficient harmonic generation in homogeneous unmagnetized plasmas.

Keywords: radially polarized beam, perturbation technique, laser-plasma interaction, second harmonic radiation generation.

1.Introduction

When intense laser pulses propagate through plasma, the electrons quiver at velocities approaching the speed of light, leading to strongly nonlinear motion. The resulting laser-plasma interaction is central to many fields, including laser-plasma acceleration (LWFA) [1- 2], attosecond laser pulse generation [3-5], self-focusing [6-7], inertial-confinement fusion [8-10], terahertz radiation generation [11-14], and harmonic generation [15-18]. Sprangle et al. performed the first theoretical evaluation of high-harmonic radiation emitted by a laser beam propagating in homogeneous plasma [19]. The seminal work of Esarey et al. further supported the study of nonlinear laser- plasma interactions for coherent high-frequency generation [20].

Additional advances include higher even and odd-harmonic efficiencies using two- color beams in gases [21], and third-harmonic generation in laser-induced plasma channels in air [22]. Subsequent studies showed that single- and two-color p-polarized beams enhance second and third harmonic generation in homogeneous plasma [23-24]. Brandi et al. analytically demonstrated second-harmonic generation (SHG) from a Hermite-Gaussian laser beam in inhomogeneous plasma [25]. Jha et al. reported SHG driven by a linearly polarized beam in magnetized homogeneous plasma [26], while another analysis found that a circularly polarized beam propagating in obliquely magnetized plasma also yields strong SHG [27]. These studies highlight the higher harmonic generation in underdense plasmas [28].

In recent years, radially polarized laser beams have attracted growing interest as drivers of higher-order harmonic radiation. Theoretical and simulation studies by Wang et al. show that a radially polarized beam, focused by an elliptical mirror, generates efficient SHG [29]. Yew et al. demonstrated that, under tight focusing, both transverse and axial field components of linearly and radially polarized beams contribute to SHG [30]. Theoretical and experimental work has confirmed that radial polarization, together with high numerical aperture focusing, enhances the axial polarization of the generated second harmonic radiation [31-32]. Experimentally, a radially polarized beam with a strong longitudinal field at focus produces significantly stronger SHG than a circularly polarized beam [33]. Mori

et al. attributed generation of second harmonic radiation to electrons oscillating at density gradients created by the laser's ponderomotive force [34]. Hashimoto et al. reported that efficiency of SHG from a self-assembled monolayer on platinum is 3.7 times stronger for a radially polarized beam than for a linearly polarized one [35].

This paper presents an analytical formulation of SHG via propagating radially polarized laser pulses through homogeneous underdense plasma and validates its findings through particle-in-cell (PIC) simulations. Section 2 derives the current density and dispersion relations for both the fundamental and second-harmonic frequencies using the Lorentz force and continuity equations. Section 3 presents closed-form expressions for the SHG amplitude and conversion efficiency and illustrates their dependence on propagation distance as well as plasma frequency normalized by laser frequency. Section 4 compares the analytical findings with simulation results, highlighting the effects of pump depletion, laser diffraction, and energy transfer to the harmonic. Section 5 summarizes the principal findings and outlines directions for future work.

2. Mathematical formulation

Consider a mildly relativistic, radially polarized laser beam propagating along z-direction in homogeneous plasma having ambient plasma density $n_o (= n_e^{(0)})$. The configuration of electric and magnetic fields are respectively given by,

$$\vec{E} = \sum_{\ell=1}^2 [\hat{r} E_{o\ell r} \cos(k_\ell z - \ell \omega_o t) + \hat{z} E_{o\ell z} \sin(k_\ell z - \ell \omega_o t)], \quad (1)$$

and

$$\vec{B} = \sum_{\ell=1}^2 \hat{\theta} E_{o\ell r} \cos(k_\ell z - \ell \omega_o t), \quad (2)$$

where $E_{o\ell r} \left[= E_o \left(\frac{r}{2r_o} \right) \exp \left(\frac{-r^2}{r_o^2} \right) \right]$ and $E_{o\ell z} \left[= E_o \left(1 - \frac{r^2}{r_o^2} \right) \exp \left(\frac{-r^2}{r_o^2} \right) \right]$ are respectively the amplitude of radial and axial components of the laser electric field while $\ell, r_o, k_\ell, \omega_o$ are frequency multiplication

factor, beam waist, wave number and fundamental frequency of the laser beam. The plasma electron velocity and density are perturbed by the passage of the radiation field and may be obtained with the help of Lorentz force and continuity equations given by,

$$\frac{\partial \vec{v}}{\partial t} = -\frac{e}{m} \left[\vec{E} + \frac{1}{c} (\vec{v} \times \vec{B}) \right] - (\vec{v} \cdot \vec{\nabla}) \vec{v}, \quad (3)$$

and

$$\frac{\partial n_e}{\partial t} + \vec{\nabla} \cdot (n_e \vec{v}) = 0, \quad (4)$$

where e , m , n_e and \vec{v} are the charge and rest mass, perturbed plasma electron density and velocity respectively.

The propagation of electric component of the laser through plasma is governed by the wave equation

$$\left(\nabla^2 - \frac{1}{c^2} \frac{\partial^2}{\partial t^2} \right) \vec{E} = \frac{4\pi}{c^2} \frac{\partial \vec{J}}{\partial t}, \quad (5)$$

where $\vec{J} (= -n_e e \vec{v})$ is the plasma electron current density which may be obtained using perturbative technique. The laser and plasma parameters are expanded upto the second order of the radiation field. With the help of Eqs. (1), (2) and (3), first order plasma electron velocities along \hat{r} and \hat{z} directions, are obtained as

$$v_r^{(1)} = \sum_{\ell=1}^2 a_{o\ell r} c \sin(k_\ell z - \ell \omega_o t), \quad (6)$$

$$v_z^{(1)} = -\sum_{\ell=1}^2 a_{o\ell z} c \cos(k_\ell z - \ell \omega_o t), \quad (7)$$

where $a_{o\ell r} = a_{oo} \left(\frac{r}{2r_o} \right) \exp(-r^2/r_o^2)$, $a_{o\ell z} = a_{oo} \left(1 - \frac{r^2}{r_o^2} \right) \exp(-r^2/r_o^2)$, and $a_{oo} [= \sum_{\ell=1}^2 (eE_o / mc\ell\omega_o)] \ll 1$. The equation governing the first order density perturbation is given by

$$\frac{\partial n_e^{(1)}}{\partial t} + \vec{\nabla} \cdot (n_e^{(0)} \vec{v}^{(1)}) = 0. \quad (8)$$

Using Eqs. (6) and (7), Eq. (8) is solved to give the first order density perturbation as,

$$n_e^{(1)} = - \sum_{\ell=1}^2 a_{o\ell z} c n_o k_\ell \frac{1}{(\ell\omega_o)} \cos(k_\ell z - \ell\omega_o t). \quad (9)$$

Substituting Eqs. (6), (7) and (9) into second order Lorentz force equation (3) leads to the radial and axial components of plasma electron velocities as

$$v_r^{(2)} = - \sum_{\ell=1}^2 a_{o\ell z} a_{o\ell r} c^2 \frac{1}{(4\ell\omega_o)} \left(\frac{\ell\omega_o}{c} + k_\ell \right) \sin 2(k_\ell z - \ell\omega_o t) \quad (10)$$

and

$$v_z^{(2)} = \sum_{\ell=1}^2 \left[-a_{o\ell r}^2 \left(\frac{\ell\omega_o}{c} \right) + a_{o\ell z}^2 k_\ell \right] c^2 \left(\frac{1}{4\ell\omega_o} \right) \cos 2(k_\ell z - \ell\omega_o t). \quad (11)$$

The current density upto the second order of radiation field is given by $\vec{J} = \vec{J}^{(1)} + \vec{J}^{(2)} = -e \left(n_o \vec{v}^{(1)} + n_e^{(1)} \vec{v}^{(1)} + n_o \vec{v}^{(2)} \right)$. Substituting the first and second order plasma electron velocities from Eqs. (6), (7), (10), (11) and first order density from Eq. (9), the radial and axial components of the first and second order current densities are respectively given by,

$$J_r^{(1)} = -n_o e c [a_{o1r} \sin(k_1 z - \omega_o t) + a_{o2r} \sin(k_2 z - 2\omega_o t)], \quad (12a)$$

$$J_r^{(2)} = n_o e c \left[\frac{a_{o1r} a_{o1z} c}{2\omega_o} \left(\frac{3k_1}{2} + \frac{\omega_o}{2c} \right) \sin 2(k_1 z - \omega_o t) \right], \quad (12b)$$

and

$$J_z^{(1)} = n_o e c [-a_{o1z} \cos(k_1 z - \omega_o t) - a_{o2z} \cos(k_2 z - 2\omega_o t)], \quad (13a)$$

$$J_z^{(2)} = n_o e c \left[\left\{ -\frac{3k_1 c}{4\omega_o} a_{o1z}^2 + \frac{1}{4} a_{o1r}^2 \right\} \cos 2(k_1 z - \omega_o t) \right]. \quad (13b)$$

It may be noted from Eqns. (12b) and (13b) that the second order current density is oscillating at the second harmonic frequency. Substituting the current density components from Eqs. (12a) and (13a) into the wave equation (Eq. (5)) and equating terms oscillating at the fundamental frequency gives the lowest order dispersion relation for the laser electric field as,

$$c^2 k_1^2 = \omega_o^2 - \omega_p^2. \quad (14)$$

Similarly, the linear dispersion relation for the second harmonic frequency can be obtained as

$$c^2 k_2^2 = 4\omega_o^2 - \omega_p^2. \quad (15)$$

3. Second harmonic generation

The amplitude of higher order second harmonic radiation is obtained by substituting the current density (Eqs. (12b) and (13b)) into the wave equation (Eq. (5)) and equating the second harmonic terms. Further, it is assumed that the second harmonic amplitude varies slowly with propagation distance ($\frac{\partial^2 a_2}{\partial z^2} \ll k_2 \frac{\partial a_2}{\partial z}$) and that a_{o1r} and a_{o1z} deplete very slightly so that the quantities a_{o1r} , a_{o1z} can be considered to be independent of z . Hence, the evolution of amplitude of r and z components of the second harmonic electric field is given by

$$\frac{\partial(a_{2r})}{\partial z} = i \frac{\omega_p^2}{2k_2 c} a_{o1r} a_{o1z} \left(\frac{3k_1}{2\omega_o} + \frac{1}{2c} \right) \exp(i \Delta k_2 z), \quad (16)$$

and

$$\frac{\partial(a_{2z})}{\partial z} = \frac{\omega_p^2}{4 i k_2 c} \left(-\frac{3k_1}{\omega_o} a_{o1z}^2 + \frac{1}{c} a_{o1r}^2 \right) \exp(i \Delta k_2 z), \quad (17)$$

where $\Delta k_2 = 2k_1 - k_2$ is the phase mismatch. While deriving Eqs. (16) and (17), the dispersion relation for the second harmonic frequency has been used. Integrating Eqs. (16) and (17) gives the r and z component of generated second harmonic amplitude as,

$$a_{2r} = i \frac{\omega_p^2}{k_2 c \omega_o \Delta k_2} a_{o1r} a_{o1z} \left(\frac{3k_1}{2} + \frac{\omega_o}{2c} \right) \exp(i \Delta k_2 z/2) \sin(\Delta k_2 z/2), \quad (18)$$

and,

$$a_{2z} = i \frac{\omega_p^2}{2 k_2 c \Delta k_2} \left(\frac{3k_1}{\omega_o} a_{o1z}^2 - \frac{1}{c} a_{o1r}^2 \right) \exp(i \Delta k_2 z/2) \sin(\Delta k_2 z/2), \quad (19)$$

It may be noted that both a_{2r} and a_{2z} are functions of r as well as z . The resultant amplitude of second harmonic radiation generated due to interaction of radially polarized laser beam with unmagnetized plasma is given by,

$$|a_2| = \sqrt{|a_{2r}|^2 + |a_{2z}|^2} = \frac{\omega_p^2}{k_2 c \Delta k_2} \left[\left\{ (a_{o1r} a_{o1z})^2 \left(\frac{3k_1}{2\omega_o} + \frac{1}{2c} \right)^2 \right\} + \left(\frac{3k_1}{2\omega_o} a_{o1z}^2 - \frac{1}{2c} a_{o1r}^2 \right)^2 \right]^{1/2} \sin(\Delta k_2 z / 2). \quad (20)$$

The second harmonic conversion efficiency, defined as the ratio of the intensity of the second harmonic and fundamental frequencies [25], is given by

$$\alpha_2 = \frac{\mu_2 |(a_2)^2|}{\mu_1 |(a_{o1})^2|}. \quad (21)$$

Here, refractive indices corresponding to the fundamental and second harmonic are $\mu_1 = (ck_1/\omega_o)$ and $\mu_2 = (ck_2/2\omega_o)$ respectively. Substituting the Eq. (20) into Eq. (21), gives second harmonic conversion efficiency as,

$$\alpha_2 = \left(\frac{\omega_p^2}{k_2 c \Delta k_2} \right)^2 \frac{\left[\left\{ (a_{o1r} a_{o1z})^2 \left(\frac{3k_1}{2\omega_o} + \frac{1}{2c} \right)^2 \right\} + \left(\frac{3k_1}{2\omega_o} a_{o1z}^2 - \frac{1}{2c} a_{o1r}^2 \right)^2 \right]}{[(a_{o1r}^2 + a_{o1z}^2)]} \sin^2(\Delta k_2 z / 2). \quad (22)$$

It may be noted that since a_{o1r} and a_{o1z} are function of r , the conversion efficiency for a given set of laser and plasma parameters varies with r as well as z .

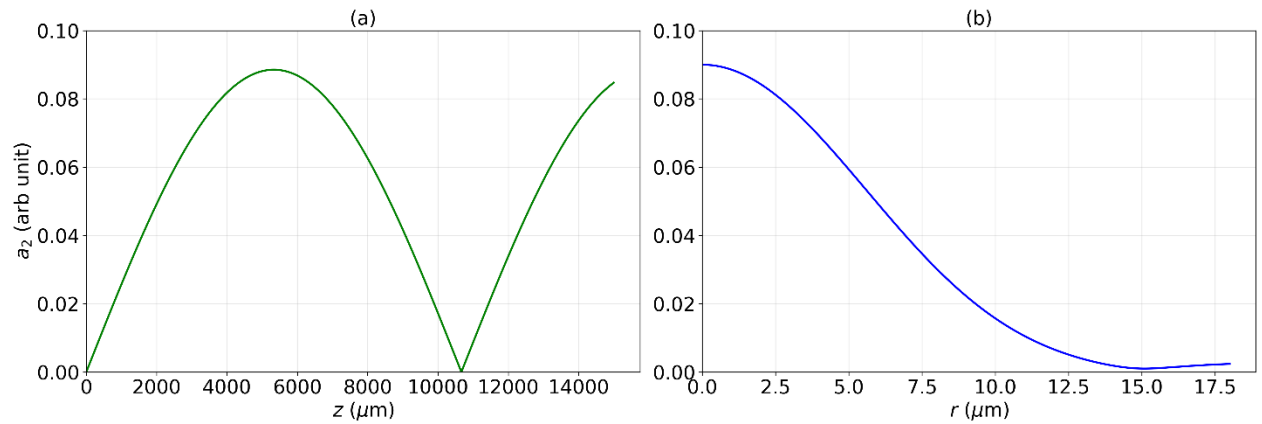


Figure 1. Variation of second harmonic amplitude a_2 (a) with respect to propagation distance z and (b) with respect to radial distance r for $a_{oo} = 0.3$, $\lambda_o = 0.8 \mu m$, $r_o = 15 \mu m$, $\omega_p/\omega_o = 0.01$, and $\omega_p = 0.23 \times 10^{14} sec^{-1}$ ($n_o = 1.75 \times 10^{24} m^{-3}$).

Analytical results are graphically depicted for the laser and plasma parameters $a_{oo} = 0.3$, $\lambda_o = 0.8 \mu m$, $r_o = 15 \mu m$, $\omega_p/\omega_o = 0.01$, and $\omega_p = 0.23 \times 10^{14} sec^{-1}$ ($n_o = 1.75 \times 10^{24} m^{-3}$). Figure 1(a) presents the analytical variation of the generated second harmonic amplitude a_2 , derived from Eq. (20), with z at $r = 1 \mu m$. It is seen that the amplitude modulates periodically with z , reaching a peak amplitude of approximately 0.09 at $z \approx 5,333 \mu m$ before decreasing due to phase mismatch. The amplitude of second harmonic radiation is maximum for $\Delta k_2 z_d/2 = \pi/2$ where $z_d = \pi/\Delta k_2$ is the detuning length. The oscillatory behavior corresponds to the coherence length, calculated analytically, which governs the periodic energy exchange between the fundamental and second harmonic fields. Similarly, the variation of amplitude with r at $z = 5,333 \mu m$. Figure 1(b) shows that $|a_2|$ decreases monotonically with increasing r , due to the combined effect of Gaussian beam profile and dependence of the laser amplitude with significant SHG confined near the axis. Figure 2 presents the variation of analytical second harmonic generation efficiency α_2 with respect to axial and radial positions for the same parameters as in Fig. 1. Figure 2 (a) exhibits a smooth sinusoidal modulation of α_2 along z , reaching a peak value of ~ 0.1 while Fig. 2(b) shows a radial variation of α_2 having maximum value (~ 0.1) near the axis.

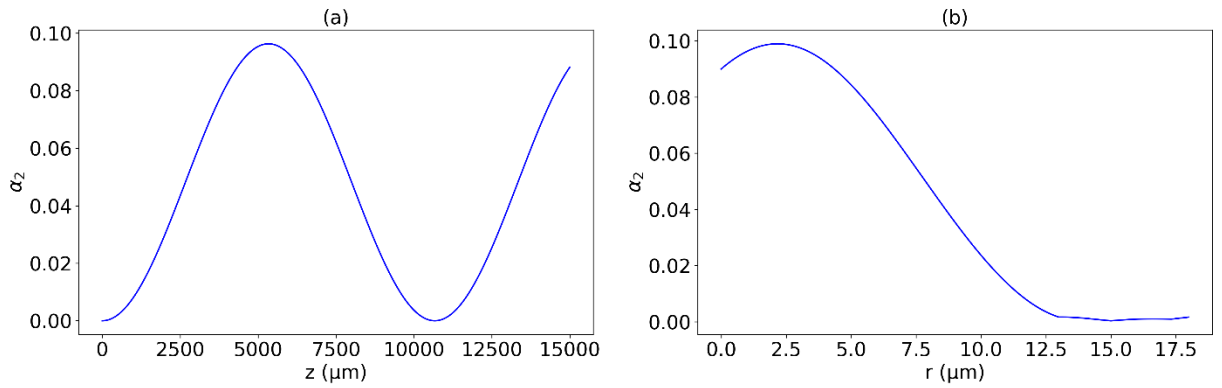


Figure 2. Variation of second harmonic efficiency α_2 (a) along z (b) along r for laser and plasma parameters as $a_{oo} = 0.3$, $\lambda_o = 0.8 \mu m$, $r_o = 15 \mu m$, $\omega_p/\omega_o = 0.01$, and $\omega_p = 0.23 \times 10^{14} sec^{-1}$ ($n_o = 1.75 \times 10^{24} m^{-3}$).

4. Simulation Results

In order to simulate second harmonic generation in homogeneous and unmagnetized plasma driven by a radially polarized laser, fully electromagnetic particle-in-cell (PIC) simulations were performed using the Fourier Bessel Particle in cell (FBPIC) code in a quasi 3D - cylindrical symmetry. The simulation domain extended from $z = -10 \mu m$ to $z = 120 \mu m$ along the longitudinal axis with $N_z = 1800$ grid cells, and up to $r = 20 \mu m$ radially with $N_r = 150$ grid points. Three azimuthal Fourier modes ($N_m = 3$) were retained to accurately capture the cylindrical symmetry of the radially polarized beam and associated harmonics. A moving window propagating at the speed of light was employed to efficiently follow the laser beam through the plasma. The temporal resolution was determined by the Courant condition and set as $\Delta t = (z_{max} - z_{min})/(N_z c) = 2 \times 10^{-16} sec$, ensuring numerical stability.

The pre-ionized plasma density ramp was initialized with a uniform electron density of $n_o = 1.75 \times 10^{24} m^{-3}$ ($\omega_p = (4\pi n_o e^2/m)^{1/2}$), extending from $z = 120 \mu m$ to $z = 250 \mu m$, and radially confined within $r \leq 18 \mu m$. To model the particle distribution in the simulation domain, 2 particles per cell were loaded along z and r , and 4 in the azimuthal (θ) direction. The continuous laser beam having laser strength parameter of $a_{oo} = 0.3$, with a beam waist of $r_o = 15 \mu m$, and wavelength $\lambda_o = 0.8 \mu m$ was focused at $z = 100 \mu m$. This configuration enabled high-resolution study of second harmonic field components under realistic experimental conditions.

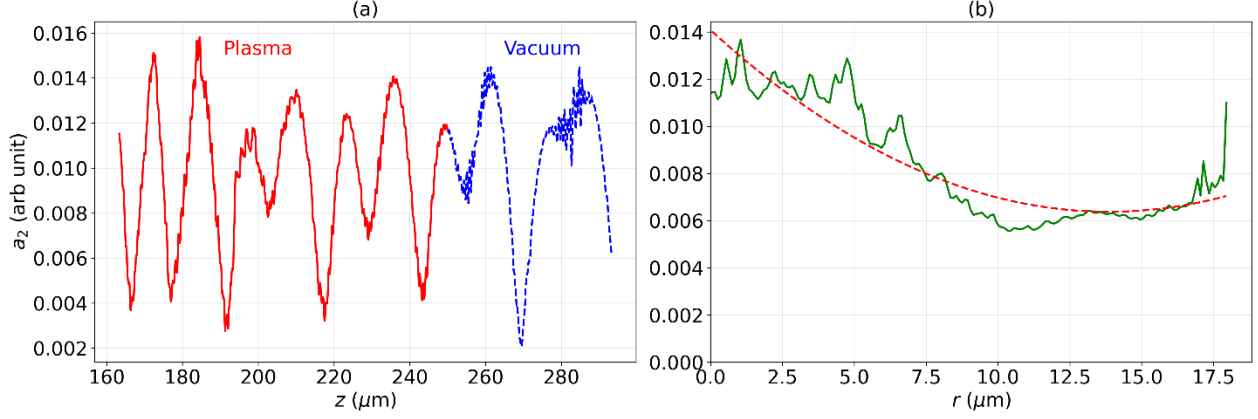


Figure 3. Variation of the second harmonic generation (SHG) amplitude a_2 for $a_{00} = 0.3$, $\lambda_0 = 0.8 \mu\text{m}$, beam waist $r_0 = 15 \mu\text{m}$, and $\omega_p/\omega_o = 0.01$. (a) a_2 versus axial distance z at fixed $r = 1 \mu\text{m}$, showing oscillatory behavior in the plasma region (solid) and in vacuum (dashed). (b) a_2 versus radial position r at fixed $z = 5,333 \mu\text{m}$, where the solid curve shows the computed profile and the dashed curve represents its best fit.

Figure 3 illustrates the variation of the second harmonic generation (SHG) amplitude a_2 with respect to the axial position (z) and radial position (r). In Fig. 3(a), the SHG amplitude is plotted along the z -axis at a fixed radial distance of $r = 1 \mu\text{m}$ near the axis. The ratio of plasma frequency to laser frequency (ω_p/ω_o) was considered to be 0.01. The solid curve represents the plasma region, while the dashed curve marks the vacuum region beyond $z = 250 \mu\text{m}$. The SHG amplitude exhibits oscillatory behavior in the plasma region as well as in the vacuum, with a peak amplitude of $a_2 \sim 0.014$. This oscillation arises on account phase-mismatch between frequencies of the laser beam and generated second harmonic radiation. In Fig. 3(b), the radial dependence of a_2 is shown at a fixed axial position $z = 5,333 \mu\text{m}$. The solid curve corresponds to the computed SHG amplitude, and the dashed line represents a second-order polynomial best fit to the simulation data. The SHG amplitude peaks near the axis with a maximum value of $a_2 \sim 0.014$ and decreases monotonically with increasing r , reflecting the radial intensity profile of the SHG radiation. It may be noted that generated second

harmonic radiation is also propagating in vacuum ($z > 250 \mu\text{m}$) and may be detected outside the plasma boundary.

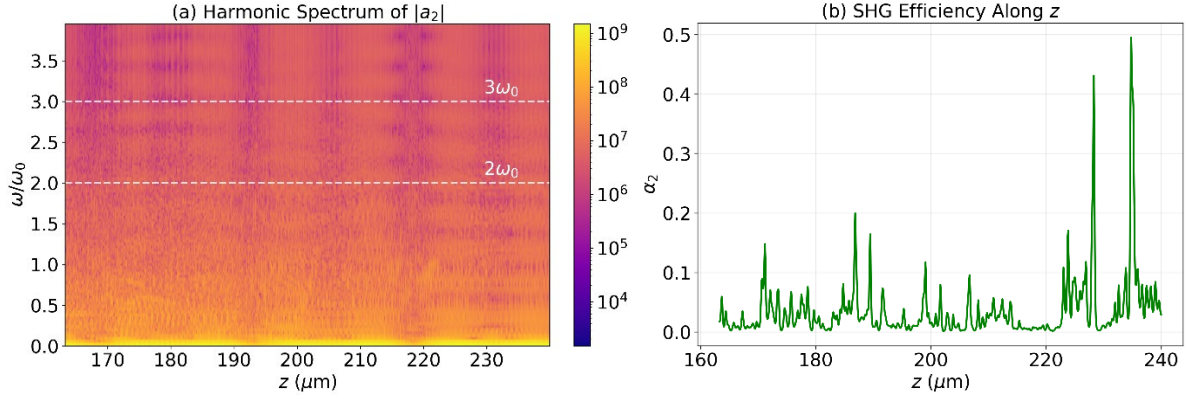


Figure 4. (a) Harmonic spectrum of the amplitude (a_2) as a function of axial position z and (b) SHG efficiency (α_2) as a function of axial position z and its best fit at $r = 1 \mu\text{m}$.

Figure 4 presents the harmonic spectrum and efficiency of generated second harmonic radiation for a radially polarized laser beam propagating in unmagnetized plasma. Fig. 4(a) shows the amplitudes of the spectrum of generated harmonics and the possibilities of enhanced second and higher harmonic frequencies. Figure 4(b) shows the efficiency (α_2) derived from the simulation data. It may be seen that the efficiency of the generated SHG follows the same trend as obtained in analytical depiction (Fig. 2).

Comparing Figs. 1 and 3, it may be noted that amplitude of the generated second harmonics derived via analytical study is greater than that obtained via simulation. In addition, detuning length obtained via analytical calculation (simulation study) is $\sim 5333 \mu\text{m}$ ($\sim 5 \mu\text{m}$). These discrepancies may be attributed to the realistic evolution of the laser beam neglected in the analytical study while being taken into consideration in the simulation study. As the laser beam propagates in plasma, it undergoes diffraction and energy depletion. These effects reduce the amplitude of the generated harmonics as seen via simulation results. These complex nonlinear dynamic effects contribute to much shorter detuning length than evaluated in analytical formulation.

5. Summary and Conclusions

The present study investigates second harmonic generation (SHG) resulting from the interaction of a radially polarized laser beam with homogeneous and unmagnetized plasma. Perturbation technique is used to obtain the current density components with the help of Lorentz force and continuity equations. The corresponding dispersion relation for the second harmonic frequencies is derived. Substitution of the radial and axial components of the current densities into the wave equation yield the respective SHG field amplitudes. The resultant amplitude of the second harmonic generated behind the laser pulse is obtained by combining the radial and axial components. Analytical findings are compared and validated with quasi-3D particle-in-cell (PIC) simulations carried out using the FBPIC code. The maximum second-harmonic amplitude obtained analytically (via simulation) is approximately 0.09 (0.014). The discrepancy in analytical and simulation results arises because the analytical formulation neglects realistic beam evolution effects such as diffraction and energy depletion, that are inherently captured in simulations. As the laser propagates through plasma, these nonlinear dynamical processes reduce the harmonic amplitude and lead to a significantly shorter detuning length than predicted analytically. Furthermore, the generated second harmonic is observed to propagate into vacuum, implying that it can be detected beyond the plasma boundary. The novelty of this study lies in demonstrating that radially polarized laser beams provide an efficient mechanism for generation of radially polarized higher-harmonic frequencies in homogeneous, unmagnetized plasma.

Data Availability Statement

Data used in the study is available on reasonable request to the Authors.

References

- [1] T. Tajima and J. M. Dawson, Laser electron accelerator, *Phys. Rev. Lett.* **43**, 267 (1979).
- [2] P. Jha, P. Kumar, A. K. Upadhyay, and G. Raj, Electric and magnetic wakefields in a

- plasma channel, *Phys. Rev. ST Accel. Beams* **8**, 071301 (2005).
- [3] P. Amendt, D. C. Eder, and S. C. Wilks, X-Ray lasing by optical-field-induced ionization, *Phys. Rev. Lett.* **66**, 2589 (1991).
- [4] A. S. Johnson et al., High-flux soft x-ray harmonic generation from ionization-shaped few-cycle laser pulses, *Sci. Adv.* **4**, 3761 (2018).
- [5] J. C. Solem et al., High brightness x-ray source for directed energy and holographic imaging applications, *IEEE J. Quantum Electron.* **25**, 2423 (1989).
- [6] C. E. Max, J. Arons, and A. B. Langdon, Self-modulation and self-focusing of electromagnetic waves in plasma, *Phys. Rev. Lett.* **33**, 209 (1974).
- [7] P. Jha et al., Self-focusing in magnetized plasma, *Phys. Plasmas* **13**, 103102 (2006).
- [8] S. C. Wilks et al., Absorption of ultra-intense laser pulses, *Phys. Rev. Lett.* **69**, 1383 (1992).
- [9] S. P. Regan et al., Laser-Plasma Interaction in long-scale-length plasmas under direct-drive National Ignition Facility conditions, *Phys. Plasmas* **6**, 2072 (1999).
- [10] M. Tabak et al., Ignition and high gain with ultrapowerful lasers, *Phys. Plasmas* **1**, 1626 (1994).
- [11] B. Xu, Y. D. Li, and L. J. Song, Simulation of THz emission from laser interaction with plasmas, *Optik* **123**, 2183 (2012).
- [12] P. Jha, A. Saroch, and R. K. Mishra, Generation of wakefields and terahertz radiation in laser-magnetized plasma interaction, *Europhys. Lett.* **94**, 15001 (2011).
- [13] S. Singh et al., Generation of tunable terahertz radiation by a laser pulse propagating in a magnetized plasma channel, *Laser Physics* **33**(7), 076001 (2023).
- [14] D. Mishra et al., Terahertz to near infrared radiation generation using two-colour counter and co-polarized laser pulses propagating in homogeneous plasma, *Physica Scripta* **98**(11), 115612 (2023).
- [15] A. McPherson et al., Studies of multiphoton production of vacuum-ultraviolet radiation in

the rare gases, *J. Opt. Soc. Am. B* **4**, 595 (1987).

- [16] A. L'Huillier and P. Balcou, Competition between ponderomotive and thermal forces in short- scale-length laser plasma, *Phys. Rev. Lett.* **69**, 1935 (1992).
- [17] P. Gibbon, High-order harmonic generation in plasmas, *IEEE J. Quantum Electron.* **33**, 1915 (1997).
- [18] X. Liu et al., Harmonic generation by an intense laser pulse in neutral and ionized gases, *IEEE Trans. Plasma Sci.* **21**, 90 (1993).
- [19] P. Sprangle and E. Esarey, Interaction of ultrahigh laser fields with beams and plasmas, *Phys. Fluids B: Plasma Physics* **4**, 2241 (1992).
- [20] E. Esarey et al., Nonlinear analysis of relativistic harmonic generation by intense lasers in plasmas, *IEEE Trans. Plasma Sci.* **21**, 95 (1993).
- [21] H. S. Brandi, P. A. Neto, and E. S. Guerra, Second-harmonic generation by intense lasers in inhomogeneous plasmas, *Phys. Rev. E* **54**(1), 1001 (1996).
- [22] P. Jha and E. Agrawal, Second harmonic generation by propagation of a p-polarized obliquely incident laser beam in underdense plasma, *Phys. Plasmas* **21**, 053107 (2014).
- [23] E. Agrawal, N. K. Verma, and P. Jha, Enhanced harmonic generation by propagation of two- color p-polarized laser beams in plasma, *Laser Part. Beams* **35**, 182 (2017).
- [24] P. Jha et al., Second harmonic generation in laser-magnetized plasma interaction, *Phys. Plasmas* **14**, 053107 (2007).
- [25] H. Yang et al., Third-order harmonic generation by self-guided femtosecond pulses in air, *Phys. Rev. E* **67**, 015401(R) (2003).
- [26] V. Malka et al., Second harmonic generation and its interaction with relativistic plasma waves driven by forward Raman instability in underdense plasmas, *Phys. Plasmas* **4**, 1127 (1997).
- [27] M. Mori, E. Takahashi, and K. Kando, Image of second harmonic emission generated from

- ponderomotively excited plasma density gradient, *Phys. Plasmas* **9**, 2812 (2002).
- [28] M. Hashimoto et al., High-sensitivity and high-spatial-resolution imaging of self-assembled monolayer on platinum using radially polarized beam excited second-harmonic-generation microscopy, *Appl. Phys. Express* **8**, 112401 (2015).
- [29] P. Sharma and P. Jha, Second harmonic generation by circularly polarized laser beam propagating in obliquely magnetized plasma, *Eur. Phys. J. D* **73**, 259 (2019).
- [30] W. Wang et al., Calculations of second harmonic generation with radially polarized excitations by elliptical mirror focusing, *J. Microsc.* **273**, 36 (2018).
- [31] E. Y. S. Yew and C. J. R. Sheppard, Second harmonic generation polarization microscopy with tightly focused linearly and radially polarized beams, *Opt. Commun.* **275**, 453 (2007).
- [32] A. Ohtsu, Y. Kozawa, and S. Sato, Calculation of second-harmonic wave pattern generated by focused cylindrical vector beams, *Appl. Phys. B* **98**, 851 (2009).
- [33] T. Ehmke et al., Molecular orientation sensitive second harmonic microscopy by radially and azimuthally polarized light, *Opt. Express* **5**, 2231 (2014).
- [34] R. M. Mart'inez-Ojeda et al., Enhancement of second harmonic microscopy images in collagen- based thick samples using radially polarized laser beams, *Opt. Commun.* **499**, 127273 (2021).
- [35] J. Mauritsson et al., Attosecond pulse trains generated using two color laser fields, *Phys. Rev. Lett.* **97**, 013001 (2006).